Vol. 6, No. 1, February 2022, pp. 79–85

Current Optics and Photonics

Regular Paper

Advantage of the Intensive Light Scattering by Plasmonic Nanoparticles in Velocimetry

Tengda Rong[1] and Quanshui Li[1,2]*

[1]*Department of Applied Physics, School of Mathematics and Physics, University of Science and Technology Beijing, Beijing 100083, China*
[2]*Beijing Key Laboratory for Magneto-Photoelectrical Composite and Interface Science, School of Mathematics and Physics, University of Science and Technology Beijing, Beijing 100083, China*

(Received October 13, 2021 : revised December 30, 2021 : accepted January 2, 2022)

Tracers are one of the critical factors for improving the performance of velocimetry. Silver and gold nanoparticles as tracers with localized surface-plasmon resonance are analyzed for their scattering properties. The scattering cross sections, angular distribution of the scattering, and equivalent scattering cross sections from 53° and 1.5° half-angle cones at 532 nm are calculated, with particle sizes in the nanoscale range. The 53° and 1.5° half-angle cones used as examples correspond respectively to the collection cones for microscope objectives in microscopic measurements and camera lenses in macroscopic measurements. We find that there is a transitional size near 35 nm when comparing the equivalent scattering cross sections between silver and gold nanoparticles in water at 532 nm. The equivalent scattering cross section of silver nanoparticles is greater or smaller than that of gold nanoparticles when the particle radius is greater or smaller than 35 nm respectively. When the radius of the plasmonic nanoparticles is smaller than about 44 nm, their equivalent scattering cross sections are at least ten times that of TiO_2 nanoparticles. Plasmonic nanoparticles are promising for velocimetry applications.

Keywords : Localized surface plasmon resonance, Noble metal nanoparticles, Particle image velocimetry, Particle tracking velocimetry, Scattering
OCIS codes : (120.7250) Velocimetry; (160.4236) Nanomaterials; (250.5403) Plasmonics; (290.5850) Scattering, particles; (290.5855) Scattering, polarization

I. INTRODUCTION

Particle-image velocimetry (PIV) [1–3], micro-particle-image velocimetry (μPIV) [4–12] and particle-tracking velocimetry (PTV) [11, 13] are powerful tools to determine the macroscopic or microscopic flow velocity in fluid applications. The tracers, optical and recording systems, and algorithms are the critical factors in applying those tools under practical working conditions [8]. The primary concerns about the tracers are focused on two aspects: the tracking capability, and the scattered or emitted light intensity. The tracking capability of the tracers dominates the accuracy of the velocimetry [1]. The relaxation time of the particle can be used to estimate this capability, and can be expressed as [1]

$$\tau_p = \frac{\rho_p d_p}{\mu_f}. \quad (1)$$

Here μ_f is the fluid-dynamical viscosity, and d_p and ρ_p are the diameter and density of the particles respectively. As shown in Eq. 1, when the size of the tracer is smaller, the relaxation time is shorter, and the tracking capability is better. Meanwhile, for the scattered or emitted light intensity

*Corresponding author: qsli@ustb.edu.cn, ORCID 0000-0002-4908-9160

Color versions of one or more of the figures in this paper are available online.

pISSN: 2508-7266 / eISSN: 2508-7274 https://doi.org/10.3807/COPP.2022.6.1.079

the size dependence conflicts with that of the relaxation time; that is, the scattering capability sharply decreases with decreasing size. The detected light intensity is determined by the scattering capability (scattering cross sections) and the laser intensity, so the size of the tracers should be chosen as a compromise [1]. Depending on the current technical levels of lasers and detectors, costs, and laser safety, the size of the tracers has a lower limit.

The tracers widely used in PIV, μPIV, and PTV include DEHS [2], water droplets [4], fluorescent polystyrene particles [7], polystyrene-latex particles [13, 14], γ-Al_2O_3 nanoparticles [9], SiO_2 particles [6, 10, 14], TiO_2 particles [10, 15], quantum dots [3], silver nanoparticles [12], and gold nanoparticles [13, 14]. For nanoparticles in a flow, the Brownian motion will cause large uncertainty in the velocimetry. Post-processing methods have been investigated to minimize the influence of Brownian motion, and satisfactory results have been obtained [13]. For those tracers other than the noble-metal nanoparticles, there is a general disadvantage that their scattering cross sections are smaller than their physical ones [16]. For quantum dots, the fluorescence is detected after the scattered light has been filtered by a dichroic mirror or short-pass filters. The absorbed light equals $I_0 C_{abs}$, where I_0 is the intensity of the incident light, and C_{abs} is the absorption cross section of the quantum dots. The dependence of the absorption cross sections on size have been investigated, and some empirical formulas have been reported [17, 18]. The absorption cross sections are smaller than the physical cross sections, following the empirical formula $C_{abs} = (5.501 \times 10^{-5})a^3$ cm^{-1} (here a is the particle radius in cm [17]), for the sizes of the quantum dots are always several nanometers. Considering that the quantum efficiency, which can be defined as the ratio of the number of emitted photons to absorbed ones, is always smaller than unity, so the equivalent cross sections (luminescence) are smaller than the physical cross sections. However, noble-metal nanoparticles with a localized surface-plasmon resonance (LSPR), called *plasmonic nanoparticles*, can be beyond this limit [16]. The collective motion of free electrons in materials driven by an external field can result in many fantastic optical effects [12–14, 16, 19–33]. If this collective motion is confined in a nanoparticle, it can be termed a localized surface-plasmon resonance (LSPR) [19]. LSPR exhibits intensive scattering when the irradiated wavelengths are in the resonance band [19–24]. Silver nanoparticles with a diameter of 35 nm [12] and gold nanoparticles [13, 14] have been used in μPIV and PTV. Furthermore, silver and gold nanoparticles have been found to exhibit nonlinear scattering behavior under intense laser irradiation [31–33]. The scattering capability of silver and gold nanoparticle is improved by increasing the incident laser intensity. Though silver and gold nanoparticles have been used as tracers in velocimetry, their optical scattering properties for PIV have not been investigated in detail.

In this paper, we investigate the scattering properties of plasmonic nanoparticles in water by simulation. The angular distribution and equivalent scattering cross sections depending on size are analyzed at 532 nm. The advantages of plasmonic nanoparticles in velocimetry are discussed.

II. MATERIALS AND METHODS

The simulations based on Mie scattering are performed using the jlmie program from Github, written by Tatsuki Hinamoto. The results from Mie theory approximate the measured extinction and scattering coefficients of a single spherical noble-metal nanoparticle [24, 25], so the simulations in this study have practical significance. The scattering spectra of the nanoparticles, the angular distributions of the scattering in the far field, and the equivalent scattering cross sections from certain cones are calculated. The refractive-index values for silver and TiO_2 are from the handbook edited by Palik [34], and that for gold is from Johnson and Christy's data [35]. Here we choose the TiO_2 particle as a reference, because it is widely used in PIV [10, 15] and there is no obvious difference in scattering properties among those tracers where the scattering cross sections are nearly equal to or smaller than the physical ones. TiO_2 is a birefringent crystal; however, in simulations the refractive index can be simplified under the average-refractive-index approximation by assuming that the particles are isotropic [26]. Water is employed as the fluid in these simulations; its refractive index is set as 1.33.

The illumination setup for μPIV and PTV can be epi-fluorescence illumination [5, 36] or dark-field illumination [4, 12]. Dark-field illumination includes not only the transmitted dark field from a condenser and the reflected darkfield from a special objective in the microscope, but also the configuration where the irradiated light does not enter the objectives or the collection lens. The common configuration for macro-PIV, in which the collection lens is out of the plane of the laser sheet, can also be used for dark-field illumination. In this study we focus on the dark-field illumination because the intense scattering of the plasmonic nanoparticles can be easily detected against the dark background.

The setup schematic for μPIV combined with a darkfield microscope can be found in ref. [12]. The illumination configuration is shown in Fig. 1(a). The light from a condenser irradiates the nanoparticles, and an objective collects the scattered light instead of the transmitted light. The collected power of the light depends on the numerical aperture (*NA*) of the objectives. Considering the symmetry along the optical axis of the condenser and the objective, we can just analyze the geometrical configuration in Fig. 1(b). The scattering cross section can be defined as

$$C = \frac{P}{I}. \tag{2}$$

Here C_{sca} is the scattering cross section (in cm^2), I_0 is the incident laser intensity (in W/cm^2), and P_{sca} is the scattered

light power (in W). The scattering cross section can be regarded as the equivalent area upon which I_0 generates the scattered light P_{sca}.

In the simulations, we use the usual conditions for microscopic velocimetry. The *NA* of an objective with 50× magnification and a dark-field condenser are 0.8 and 0.9, which correspond to half angles of 53° and 64° respectively. The collected light in the far field from the objectives can be obtained from the collection cone with a half angle of 53°. The collection schematic for macro-PIV is shown in Fig. 1(c). The half angle of the collection cone is set as 1.5° for instance, which corresponds to the collection cone from a camera lens 50 mm in diameter, about 1 m away.

Here we define the equivalent scattering cross section $C_{sca,e}$. The power of the scattered light $P_{sca,e}$ in that cone is

$$P_{sca,e} = I_0 C_{sca,e}. \quad (3)$$

If the linearly polarized light passes through the dark-field condenser and irradiates the nanoparticles, due to the rotational symmetry of the mirrors in the condenser the polarization of the light irradiated on the nanoparticles should rotate 360° about the propagation direction, so the average equivalent scattering cross-section should be $0.5(C_{sca,p} + C_{sca,s})$, in which *p* means the polarization parallel to the incident plane formed by the propagation direction (*k*) and optical axis (*c*), and *s* is normal to the incident plane. We first calculate the two polarization conditions shown in Fig. 1(b), and then average them.

III. RESULTS

The far-field scattering cross sections of silver, gold, and TiO_2 nanoparticles of different sizes are shown in Fig. 2. For the silver and gold nanoparticles, enhanced scattering is seen in the resonance band. Scattering strongly depends on the size of the particle, and the scattering cross sections of the nanoparticles sharply decrease with decreasing size. The contribution of scattering to the total extinction also decreases, and that of absorption increases, with decreasing size.

We focus on the scattering properties at a wavelength of

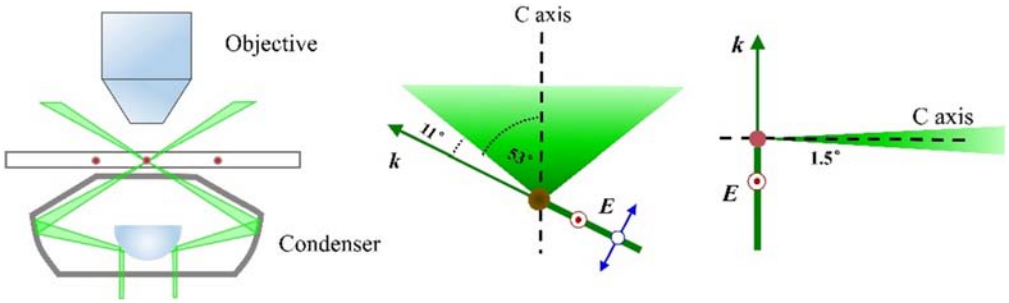

(a) (b) (c)

FIG. 1. The schematic for dark-field illumination: (a) μPIV configuration, (b) the polarization of the light, and the related collection cone of the scattered light, and (c) the collection cone for macro-PIV. *k* and *E* indicate the propagation of the light and the polarization direction respectively. The red and blue arrows in (b) represent *s* and *p* polarizations respectively. The C axis represents the optical axis of the objective and condenser, and the optical axis of the collection lens in (b). The angle between the C axis and the direction of light propagation is 64°. The angles 53° and 1.5° represent the half angles of the respective collection cones.

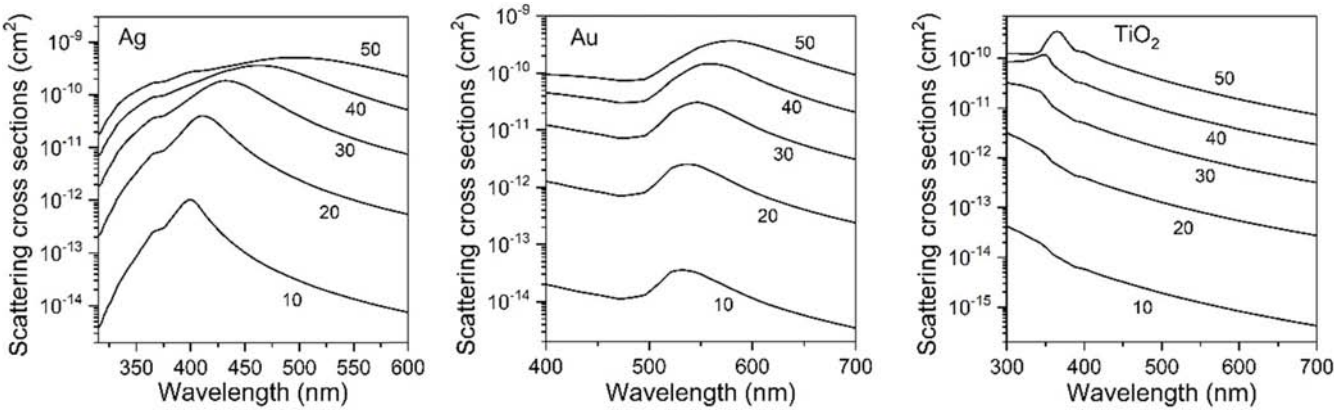

(a) (b) (c)

FIG. 2. Scattering cross sections of (a) silver nanoparticles, (b) gold nanoparticles, and (c) TiO_2 nanoparticles. The log scale is used to plot the scattering cross sections. The sizes of the nanoparticles are labeled near the curves (in units of nm).

532 nm because 532-nm lasers are popular for PIV, due to the low cost and sophisticated techniques. The angular distributions of the scattering from the silver, gold, and TiO_2 nanoparticles at 532 nm are shown in polar coordinates in Fig. 3. The propagation direction of the light is along the *z* axis, and the polarization is along the *x* axis. The angular distributions in the *xy* plane, *yz* plane, and *xz* plane are obtained. The angular dependence of the scattered light is not obvious in the *yz* plane for the silver and gold nanoparticles, except for the 50-nm gold particles. The scattered light at different angles is similar, including forward scattering and backward scattering, while for the TiO_2 nanoparticles the forward scattering is a little stronger than the backward. This asymmetry of forward and backward scattering vanishes as the size of the nanoparticles decreases. The scattered light in the *xz* and *xy* planes exhibits strong

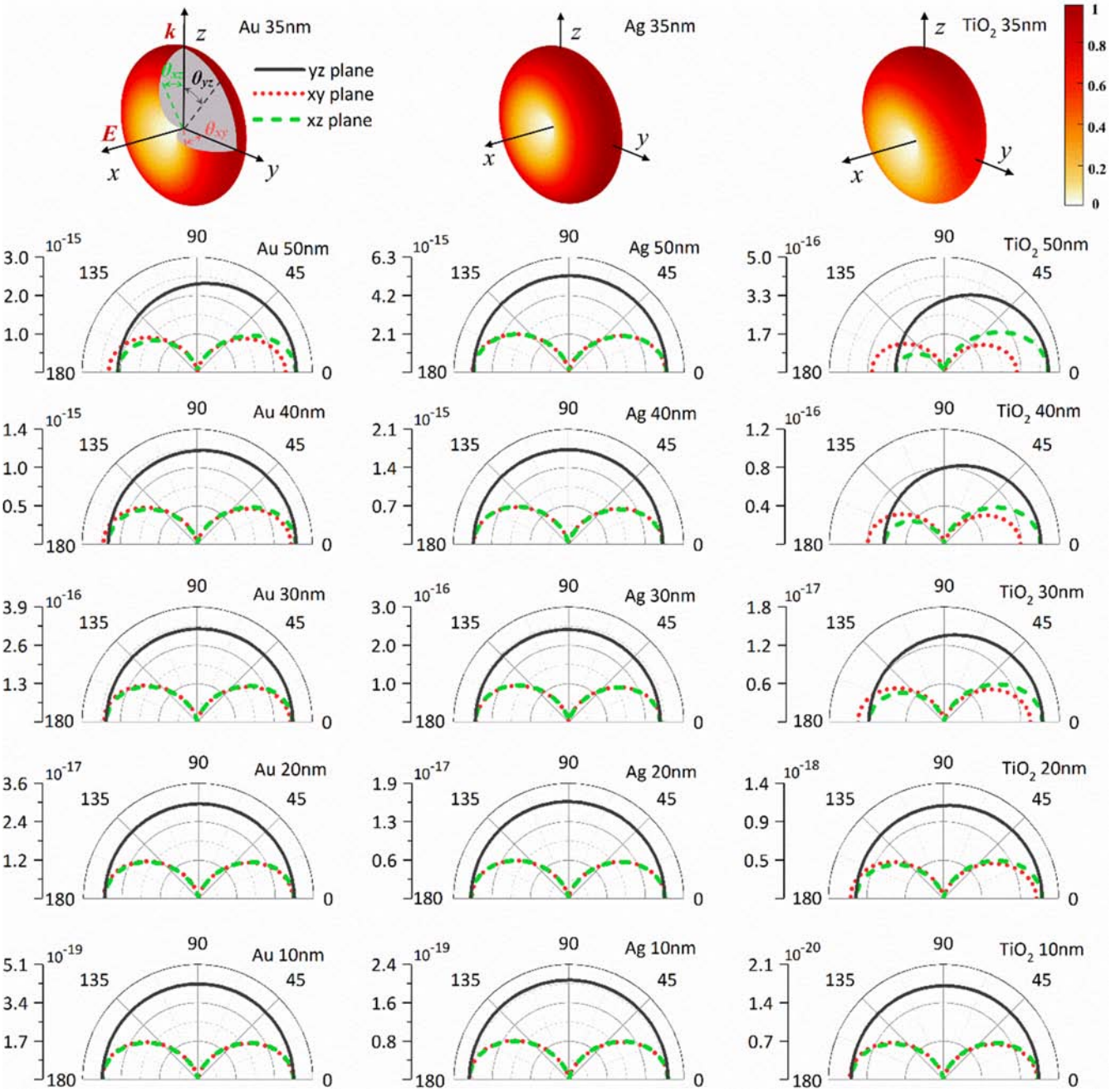

FIG. 3. The angular distribution of the scattering for silver, gold, and TiO_2 nanoparticles, from 0°–180°, at 532 nm. The definitions of the angles in the three-dimensional scattering graph are shown in the first row. The color represents the normalized scattering cross section per unit area. The propagation direction (*k*) is along the z axis, and the direction of the polarization (*E*) is along the *x* axis. Scattering in the *x*-*y* plane, *y*-*z* plane, and *x*-*z* plane is drawn in red, black, and green lines respectively. The sizes and compositions of the nanoparticles are labeled at the top right corner of each subfigure. Here the value of the polar radius represents the scattering cross section per unit area (cm^2/cm^2, dimensionless), 1 meter away from the nanoparticles.

angular dependence. The scattering decreases when the angle approaches 90°, which means that the scattered light is minimal along the polarization direction. Thus the polarization of the incident laser should be adjusted according to the position of the collection optics. Because the collection solid angle of the macroscopic measurement is small, the collection optics should be around the direction normal to the polarization direction and the propagation direction. In the *yz* plane the scattered light from the silver and gold nanoparticles is greater than that from TiO_2 nanoparticles of the same size.

The collected light is within the particular solid angle determined by the aperture of the collection lens. The equivalent scattering cross section is the scattering capability of the nanoparticle combined with the collection optics. For μPIV applications, the equivalent scattering cross sections of the silver and gold nanoparticles for a half angle of 53° are shown in Figs. 4(a) and 4(b). The equivalent cross sections increase with increasing size. Similar behavior is also found for the 1.5° half-angle cone, as shown in Fig. 4(c). The ratio for silver and gold with varying size is shown in Fig. 4(d). In this figure, we can see that the scattering cross section of the gold nanoparticles is greater than that of the silver nanoparticles below about 35 nm in radius, for the 53° and 1.5° half-angle cones. Beyond 35 nm, the scattering cross section of the silver nanoparticles is greater. Furthermore, we found the ratio of the total scattering cross sections shows similar results. The ratios for the silver and the gold nanoparticles to the TiO_2 nanoparticles are shown in Fig. 4(e). A peak is found at about 40 nm and 19 nm for Ag/TiO_2 and Au/TiO_2 respectively. In general, the scattering capability of both silver and gold nanoparticles is greater than that of TiO_2 nanoparticles. The equivalent scattering cross section of the silver nanoparticles is at least ten times that of the TiO_2 nanoparticles, when the size is smaller than about 54 nm; for the gold nanoparticles, this size is about 44 nm. As shown in Figs. 4(a)–4(c), the scattering cross section sharply decreases with decreasing size, so the scattering capability of the tracers and the threshold of the detector should be considered together. If the detector is sensitive enough, smaller gold nanoparticles are desirable; otherwise, the bigger silver nanoparticles are appropriate.

Plasmonic nanoparticles have been found to exhibit nonlinear scattering effects [31–33]. Their scattering cross sections vary with incident intensity: At high intensity, the scattering cross section is greater than that at low intensity [31–33]. This nonlinear scattering will benefit the detection of the scattered light. However, the nonlinear scatter-

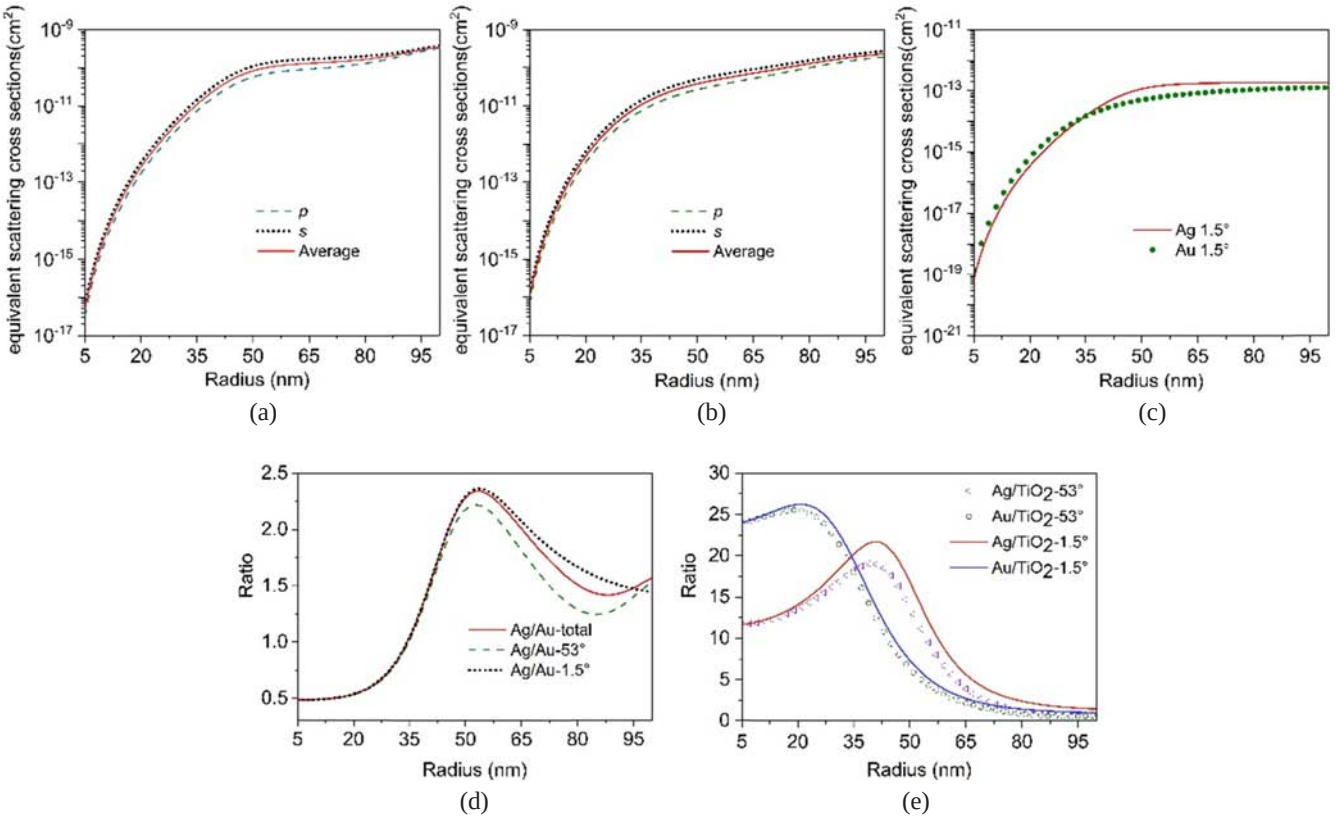

FIG. 4. The equivalent scattering cross sections of (a) silver and (b) gold nanoparticles, for a half angle of 53°. (c) The equivalent scattering cross sections of silver and gold nanoparticles for a half angle of 1.5°. (d) The ratio of the average equivalent scattering cross sections of silver and gold nanoparticles at half angles of 53° and 1.5°, and the ratio of total scattering cross sections. (e) The ratio of the equivalent scattering cross sections of silver and TiO_2 nanoparticles, and of the gold nanoparticles and the TiO_2, at half angles of 53° and 1.5°. The radius ranges from 5 to 100 nm. The incident wavelength is 532 nm.

ing is complex, for the scattering cross section is found to decrease and then increase with incident intensity, under irradiation by a continuous laser [31]. Therefore, for application in PIV the nonlinear responses and their mechanisms for plasmonic nanoparticles under both pulsed and continuous lasers should be investigated in detail. These nonlinear effects are very promising for PIV applications.

Temperature is an important factor in the optical properties of silver and gold nanoparticles. In principle, the extinction (including absorption and scattering) coefficients of nanoparticles will decrease with increasing temperature [21–23], and experimental results show that the extinction or scattering coefficients of silver and gold nanoparticles at 532 nm slightly decrease, from room temperature to about 70 ℃ [22,23]. The temperature influence is small for metal nanoparticles in liquid, in the usual temperature range.

The advantage of plasmonic nanoparticles is the enhanced scattering arising from the localized surface-plasmon resonance. In the nanoscale range, intense scattering can be obtained by employing silver or gold nanoparticles of the desired sizes. The intense scattering cross sections of the tracers will decrease the required power of the laser and sensitivity of the detectors. The optical results of this study can be used as a reference for the choice of tracers and laser parameters in the linear optical regime, such as the power (energy) and the polarization.

The silver and gold nanoparticles have plasmonic resonance bands, so as tracers they will exhibit more intense scattering when the laser works at the resonance wavelength. It is worth noting that the metal nanoparticles have enhanced photothermal properties, and so can be used to perform flash-activated ignition [19]. Thus plasmonic nanoparticles should not be used as tracers in flammable fluid. In summary, the intense scattering by plasmonic nanoparticles is of great advantage in PIV applications.

IV. CONCLUSION

Toward applications in velocimetry, the scattering spectra, angular distributions of scattering, and equivalent scattering cross-sections have been calculated for silver, gold, and TiO_2 nanoparticles in water. The equivalent scattering cross sections of the silver and gold nanoparticles are calculated for 53° and 1.5° half-angle cones at 532 nm, with the sizes of the nanoparticles in the nanoscale range. The equivalent scattering cross sections of the silver nanoparticles are greater than those of the gold nanoparticles, when particle size is larger than 35 nm. When the particles are smaller than 35 nm, the equivalent scattering cross section of the gold particles is greater than that of the silver. When the radius of the plasmonic nanoparticles is smaller than about 44 nm, the equivalent scattering cross sections of the plasmonic nanoparticles are at least 10 times that of TiO_2 nanoparticles. Therefore the intense scattering from plasmonic nanoparticles will benefit PIV applications.

FUNDING

Fundamental Research Funds for the Central Universities (FRF-BR-19-002B); Scientific Research Foundation for the Returned Overseas Chinese Scholars (48th).

ACKNOWLEDGMENT

Q. Li received those fundings from his University and Ministry of Education of the People's Republic of China, respectively. T. Rong's contributions are idea, simulation, visualization and analysis. Q. Li's contributions are idea, methodology, and analysis.

REFERENCES

1. A. Melling, "Tracer particles and seeding for particle image velocimetry," Meas. Sci. Technol. **8**, 1406–1416 (1997).
2. M. Braun, W. Schröder, and M. Klaas, "High-speed tomographic PIV measurements in a DISI engine," Exp. Fluids **60**, 146 (2019).
3. S. Pouya, M. Koochesfahani, P. Snee, M. Bawendi, and D. Nocera, "Single quantum dot (QD) imaging of fluid flow near surfaces," Exp. Fluids **39**, 784–786 (2005).
4. D. Malsch, M. Kielpinski, R. Merthan, J. Albert, G. Mayer, J. M. Köhler, H. Süße, M. Stahl, and T. Henkel, "μPIV-analysis of Taylor flow in micro channels," Chem. Eng. J. **135**, S166–S172 (2008).
5. J. G. Santiago, S. T. Wereley, C. D. Meinhart, D. J. Beebe, and R. J. Adrian, "A particle image velocimetry system for microfluidics," Exp. Fluids **25**, 316–319 (1998).
6. M. Shimura, S. Yoshida, K. Osawa, Y. Minamoto, T. Yokomori, K. Iwamoto, M. Tanahashi, and H. Kosaka, "Micro particle image velocimetry investigation of near-wall behaviors of tumble enhanced flow in an internal combustion engine," Int. J. Eng. Res. **20**, 718–725 (2019).
7. J. Westerweel, P. F. Geelhoed, and R. Lindken, "Single-pixel resolution ensemble correlation for micro-PIV applications," Exp. Fluids **37**, 375–384 (2004).
8. M. Raffel, C. E. Willert, S. T. Wereley, and J. Kompenhans, *Particle Image Velocimetry*, 2th ed. (Springer-Verlag, Germany. 2007).
9. P. A. Walsh, V. M. Egan, and E. J. Walsh, "Novel micro-PIV study enables a greater understanding of nanoparticle suspension flows: nanofluids," Microfluid. Nanofluidics **8**, 837–842 (2010).
10. M. Mujat, R. D. Ferguson, N. Iftimia, D. X. Hammer, I. Nedyalkov, M. Wosnik, and H. Legner, "Optical coherence tomography-based micro-particle image velocimetry," Opt. Lett. **38**, 4558–4561 (2013).
11. S. J. Williams, C. Park, and S. T. Wereley, "Advances and applications on microfluidic velocimetry techniques," Microfluid. Nanofluid. **8**, 709–726 (2010).
12. Z. Zhang, Q. Li, S. S. Haque, and M. Zhang, "Far-field plasmonic resonance enhanced nanoparticle image velocimetry within a microchannel," Rev. Sci. Inst. **82**, 023117 (2011).

13. Y. Matsuura, A. Nakamura, and H. Kato, "Nanoparticle tracking velocimetry by observing light scattering from individual particles," Sens. Actuators B Chem. **256**, 1078–1085 (2018).
14. Y. Matsuura, A. Nakamura, and H. Kato, "Determination of nanoparticle size using flow particle tracking method," Anal. Chem. **90**, 4182–4187 (2018).
15. Y. X. Zhao, S. H. Yi, L. F. Tian, and Z. Y. Cheng, "Supersonic flow imaging via nanoparticles," Sci. China Technol. Sci. **39**, 3640 (2009).
16. T. Ming, H. J. Chen, R. B. Jiang, Q. Li, and J. F. Wang, "Plasmon-Controlled Fluorescence: Beyond the Intensity Enhancement," J. Phys. Chem. Lett. **3**, 191–202 (2012).
17. C. A. Leatherdale, W.-K. Woo, F. V. Mikulec, and M. G. Bawendi, "On the absorption cross section of CdSe nanocrystal quantum dots," J. Phys. Chem. B **106**, 7619–7622 (2002).
18. P. Yu, M. C. Beard, R. J. Ellingson, S. Ferrere, C. Curtis, J. Drexler, F. Luiszer, and A. J. Nozik, "Absorption cross-section and related optical properties of colloidal InAs quantum dots," J. Phys. Chem. B **109**, 7084–7087 (2005).
19. J. E. Abboud, X. Chong, M. Zhang, Z. Zhang, N. Jiang, S. Roy, and J. R. Gord, "Photothermally activated motion and ignition using aluminum nanoparticles," Appl. Phys. Lett. **102**, 023905 (2013).
20. X. Zhang and Q. Li, "Forced damped harmonic oscillator model of the dipole mode of localized surface plasmon resonance," Plasmonics **16**, 1525–1536 (2021).
21. L. K. Sørensen, D. E. Khrennikov, V. S. Gerasimov, A. E. Ershov, M. A Vysotin, S. Monti, V I. Zakomirnyi, S. P. Polyutov, H.Ågren, and S. V. Karpov, "Thermal degradation of optical resonances in plasmonic nanoparticles," Nanoscale **14**, 433–447 (2022).
22. S. Link and M. A. El-Sayed, "Size and temperature dependence of the plasmon absorption of colloidal gold nanoparticles," J. Phys. Chem. B **103**, 4212–4217 (1999).
23. T. P. Otanicar, B. T. Higgins, S. Brunter, P. E. Phelan, L. Dai, and R. Swaminathan, "Temperature dependent optical properties of nanoparticle suspensions," in *Proc. ASME 2012 Heat Transfer Summer Conference collocated with the ASME 2012 Fluids Engineering Division Summer Meeting and the ASME 2012 10th International Conference on Nanochannels, Microchannels, and Minichannels* (Puerto Rico, USA, Jul. 2012).
24. A. M. Olaizola, "Photothermal determination of absorption and scattering spectra of silver nanoparticles," Appl. Spectrosc. **72**, 234–240 (2018).
25. D. D. Evanoff and G. Chumanov, "Size-controlled synthesis of nanoparticles. 2. Measurement of extinction, scattering, and absorption cross sections," J. Phys. Chem. B **108**, 13957–13962 (2004).
26. Q. Li and Z. Zhang, "Broadband tunable and double dipole surface plasmon resonance by TiO_2 Core/Ag shell nanoparticles," Plasmonics **6**, 779–784 (2011).
27. Y. Lyu, J. Ruan, M. Zhao, R. Hong, H. Lin, D. Zhang, and C. Tao, "Enhancement of photoluminescence by Ag localized surface plasmon resonance for ultraviolet detection," Curr. Opt. Photonics **5**, 1–7 (2021).
28. G. Seok, S. Choi, and Y. Kim, "Single-pixel autofocus with plasmonic nanostructures," Curr. Opt. Photonics **4**, 428–433 (2020).
29. A. Farmani, "Three-dimensional FDTD analysis of a nanostructured plasmonic sensor in the near-infrared range," J. Opt. Soc. America B **36**, 401–407 (2019).
30. A. Farmani and A. Mir, "Graphene sensor based on surface plasmon resonance for optical scanning," IEEE Photonics Technol. Lett. **31**, 643–646 (2019).
31. Y.-T. Chen, P.-H. Lee, P.-T. Shen, J. Launer, R. Oketani, K.-Y. Li, Y.-T. Huang, K. Masui, S. Shoji, K. Fujita, and S.-W. Chu, "Study of nonlinear plasmonic scattering in metallic nanoparticles," ACS Photonics **3**, 1432–1439 (2016).
32. L. Polavarapu, Q. H. Xu, M. S. Dhoni, and W. Ji, "Optical limiting properties of silver nanoprisms," Appl. Phys. Lett. **92**, 263110 (2008).
33. V. Liberman, M. Sworin, R. P. Kingsborough, G. P. Geurtsen, and M. Rothschild, "Nonlinear bleaching, absorption, and scattering of 532-nm-irradiated plasmonic nanoparticles," J. Appl. Phys. **113**, 053107 (2013).
34. E. D. Palik, *Handbook of Optical Constants of Solids* (Academic Press, USA. 1985).
35. P. B. Johnson and R. W. Christy, "Optical constants of the noble metals," Phys. Rev. B **6**, 4370–4379 (1972).
36. M. G. Olsen and R. J. Adrian, "Out-of-focus effects on particle image visibility and correlation in microscopic particle image velocimetry," Exp. Fluids **29**, S166–S174 (2000).